해부 · 생물인류학 제 32 권 제 4 호
Anat Biol Anthropol Vol. 32, No. 4 (2019) pp. 129~139
https://doi.org/10.11637/aba.2019.32.4.129

Check for updates

Original Article

Metformin-loaded Citric Acid Cross-linked Agarose Films in the Prevention of Postoperative Abdominal Adhesion

Ji Hyun Moon[1], Jong Ho Park[2], Ji Heun Jeong[1], Nak Song Sung[3], Young Gil Jeong[1], Ki Chang Song[2], Jong Pil Ahn[4], Nam-Seob Lee[1], Seung Yun Han[1]

[1]*Department of Anatomy, College of Medicine, Konyang University*
[2]*Department of Biomedical Material, College of Medical Engineering, Konyang University*
[3]*Department of General Surgery, Konyang University Hospital*
[4]*Korea Institute of Ceramic Engineering and Technology*

Abstract : Postoperative abdominal adhesion (PAA) causes significant long-term postoperative morbidity. Although numerous physical anti-adhesion barriers (AAB) are used as therapeutical interventions, none of them has achieved sustained success. As a potential strategy to overcome the limitations, drug-eluting AAB have attracted scientific attention. Here, we produced agar films (AF) chemically cross-linked with different concentrations of citric acid (CA) and we measured the physicochemical properties such as crosslinking strength, swelling ratio, hydrophilicity, and biodegradability of the yielded CA-AFs. Next, Metformin (MET), an anti-diabetic drug with anti-proliferative and anti-inflammatory properties, was loaded in the CA-AFs yielding the MET-loaded CA-AF (MET@CA-AF) and the time-dependent MET release was monitored. Based on their physicochemical properties, MET@CA-AF containing 20% CA appeared a promising AAB candidate and was further used in an *in vivo* study. Mouse models of PAA were established with cecum abrasion and the MET@CA-AF and CA-AF were applied between the injured interfaces. At postoperative day 14, the therapeutic efficacies were analyzed by using clinical adhesion scoring and quantification of collagen-I and fibroblasts in adhesion interfaces. The results showed that applications of MET@CA-AF or CA-AF for 14 days significantly attenuated the clinical adhesion score and thickness of adhesion interface. Furthermore, when compared with the group with operation, the groups with MET@CA-AF or CA-AF exhibited the significant attenuation in PAA-associated myofibroblast activation in adhesion interface. Importantly, these attenuations were significantly more intensified in the group with MET@CA-AF than in the group with CA-AF. Based on our data, we anticipate that MET@CA-AF, a novel synthesized drug-eluting AAB, can protect against PAA by exerting the dual role of physical barrier and MET-based pharmaceutic.

Keywords : Agarose, Anti-adhesion barriers, Metformin, Postoperative abdominal adhesion

INTRODUCTION

Postoperative abdominal adhesion (PAA) is an inevitable consequence of intra-abdominal surgeries [1]. PAA is a major cause of morbidity resulting in various complications, many of which can persist for several years after the initial operation [2,3]. To date, the PAA-associated complications,

This research was supported by grants from the Korea Research Foundation (NRF2019R1C1C1002294 and 2017R1D1A3B040348).
The author(s) agree to abide by the good publication practice guideline for medical journals.
The author(s) declare that there are no conflicts of interest.
Received: October 21, 2019; **Revised:** October 23, 2019;
Accepted: October 24, 2019
Correspondence to: Nam-Seob Lee, Ph.D (Department of Anatomy, College of Medicine, Konyang University), Seung Yun Han, M.D, Ph.D (Department of Anatomy, College of Medicine, Konyang University)
E-mail: nslee@konyang.ac.kr, jjzzy@konyang.ac.kr

ISSN 2671-566X (Online) · ISSN 2671-5651 (Print)

e.g., acute small bowel obstruction, pelvic or abdominal pain, and infertility, continue to challenge human healthcare worldwide without any apparent therapeutic options [3,4].

Up to date, the application of physical anti-adhesion barriers (AAB) has been widely accepted as the optimal strategy against PAA [5]. In particular, polymeric hydrogel-based AABs have attracted attention in both preclinical studies and clinical trials [6]. Hydrogels are a special class of 3-dimensional polymeric network, which can retain significant body fluids while maintaining their physical integrity [7]. Currently, several commercial hydrogel-based AABs including Adept® (Baxter) and Sepracoat® (Genzyme) as solutions and Seprafilm® (Genzyme) and Surgiwrap® (MAST Biosurgery) as solid membranes are commercially available with different degrees of success [3,8,9]. However, all these pure AABs failed to protect against PAA because they fail to address the basic biological problems including the difficulties in the control of their biocompatibility and biodegradability [10].

In recent years, researchers in this field have hypothesized that the limitations of AABs could be overcome by combining their role as a physical barrier with a potential pharmacological potency [11,12]. As such, the hydrogels were shown to act not only as a physical barrier at the surgical wound, but also as a drug delivery system [11,13]. Among the various drugs that have been used to target different steps in the PAA pathophysiological mechanism, the anti-proliferative drug paclitaxel, was shown to attenuate PAA symptoms in rat model when loaded in a cross-linked hyaluronic acid film [14]. In addition, Ancrod, a fibrinolytic agent made from Malayan pit viper venom, in combination with a hydrogel has been revealed to exert the therapeutic effect in PAA rat model [15].

In line with the hypothesis described above, this study tested the therapeutic potential of a "drug-eluting" hydrogel-based AAB, which consists of agarose and Metformin (MET). Agarose, originating from specific algae, is a highly hydrophilic polymer, which has a unique gel property and favorable biocompatibility. Therefore, agarose is attracting considerable interest with its economic and environmental benefits [16]. On the other hand, the drug for diabetes mellitus, MET has anti-proliferative [17] and anti-inflammatory effects [18].

In this study, we enhanced the physical strength of agarose, thereby forming agarose films (AF) by using citric acid (CA) as a cross-linking agent. The cross-linking occurred by reaction between the carboxyl groups in CA and the hydroxyl group in ethylene glycol present in the agarose [19]. We characterized the physicochemical properties of the resulting CA-AFs, which contained different concentrations of CA. Next, we loaded MET in the CA-AFs, yielding MET@CA-AF, and obtained the releasing profiles of MET from MET@CA-AF. To test whether the application of MET@CA-AF can confer the prevention against the PAA pathogenesis, we employed the *in vivo* PAA models, which was established with mice with cecal abrasion operation. By quantification of the clinical adhesion severity and the histopathological changes at postoperative day 14th, we examined the preventive effect of MET@CA-AF and the possible mechanisms in relation to inhibition of myofibroblast activation, a major culprit of PAA pathogenesis.

MATERIALS AND METHODS

Chemicals

Agarose (Analytical grade) was purchased from Promega (Madison, WI, USA). Glycerin was purchased from Daejung (Busan, Korea). Hematoxylin and Eosin (H-E) staining kit, citric acid, and Metformin hydrochloride were purchased from Sigma Aldrich (St. Louis, MO, USA). Masson's trichrome staining kit, rabbit polyclonal anti-collagen I (Cat. #ab34710) and mouse monoclonal anti-vimentin (Cat. #Ab8978) antibodies were purchased from Abcam (Cambridge, UK).

Synthesis of CA-AFs

In 250 mL Erlenmeyer flasks, 3 g agarose and 0.9 g glycerin were dissolved in 30 mL of phosphate-buffered saline (PBS, pH 7.4). A viscous solution was obtained by complete dissolving in a microwave generator set at 800 W for 10 min. Mechanical cross-linking was performed by freezing the solution at around −2°C for 30 min. Next, the mixture was heated again in a microwave. For chemical cross-linking, the viscous solution was mixed with different concentrations of citric acid (CA) (0, 10, and 20% w/w to amount of agarose) by using a spatula. Different CA-AFs were obtained by casting 2 g of the resulting mixtures in films and air-drying them. The CA-AFs were named C0, C10, and C20 according to the % content of CA.

Fourier transform infrared spectroscopy

To confirm the existence of ester-bond formation, an indicator of crosslinking, Fourier transform infrared (FT-IR) spectra of dried CA-AFs were recorded using FT-IR Cary 630 (Agilent, Santa Clara, CA, USA) in wavenumber range from 400 cm^{-1} to 4000 cm^{-1}.

Swelling properties

Swelling behavior of C0, C10, and C20 was studied as follows. Small strips of each film (1 × 2 cm in size) were cut and their initial weights (W_0) were measured. The strips were immersed in PBS maintained at 37°C and pH 7.3. After 24 h, the strips were taken out, wiped with filter paper, and their weights after swelling (W_t) were measured. The swelling ratio was obtained using the following equation: W_t / W_0.

Contact angle measurement

A contact angle meter (PheonixMini-10; Suwon, Gyeonggi-do, Korea) was used to measure the hydrophilicity of the C0, C10, and C20. Using a zoom microscope, the image of the surface was enlarged to an optimum magnification and the contact angle was measured by dropping 2 mL of water droplets on each surface of the samples.

In vitro biodegradation assay

To speculate the in-body decomposition behavior of the CA-AFs, *in vitro* biodegradation assay was performed. In brief, the C0, C10, and C20 (n = 14 per each) were cut into 1 × 2 cm pieces and each W_0 was measured. Then, the films were immersed in 10 mL of PBS maintained at 37°C and pH 7.3 while stirring continuously. In the course of 14 days, every day 1 film was withdrawn from PBS and dried for 24 h in an oven kept at 37°C. The completely dried films were weighed. The resulting data were plotted as means of weight loss (%) per W_0 of each films.

Synthesis of MET@CA-AF and drug release assay

MET was loaded in the hydrogel films using the swelling equilibrium method [20]. In brief, pre-weighed C0, C10, and C20 films (~2 g) were mixed with 50 mg MET dissolved in 20 mL PBS. After 2 h, the films were dried in an oven at 40°C for 24 h to yield the MET@CA-AFs with different concentrations of CA. To determine the amount of the loaded drug, the films were cut into small pieces, weighed, and immersed in 50 mL PBS. The dispersion was stirred on a magnetic stirrer at 100 rpm for 24 h and the amount of MET was determined using a UV/Vis spectrophotometer (Shimadzu, Kyoto, Japan) at λ_{max} 234 nm. To determine that amount of released MET, we kept the MET@CA-AFs with different concentrations of CA (~2 g) in 50 mL PBS (pH 7.4) at 37°C. At different time points, 2 mL were withdrawn and 2 mL fresh PBS were added. The amount of released MET was determined using a UV/Vis spectrophotometer at λ_{max} 234 nm up to 1500 min.

Animals

A total of 32 C57BL/6 mice (male, 10 week old) were purchased from Samtako (Osan, Korea). The mice were housed under constant temperature (23°C) and humidity (45~55%) with a 12 h light/dark cycle and free access to food and water. Experiments were carried out according to the Guide for Care and Use of Laboratory Animals (2011, National Institutes of Health, Bethesda, MD, USA) [21] and were approved by the Institutional Animal Care and Use Committee (IACUC) of Konyang University.

Surgical procedures and drug application

Mice were divided in 4 groups (n = 8 per each) as follows: CTRL, the group of controls; OP, the group operated with cecal abrasion, a surgical method for modelling PAA [22]; CA-AF and MET@CA-AF, the groups with the operations and concomitant applications of CA-AF or MET@CA-AF, respectively. At that time, concentration of CA for both CA-AF and MET@CA-AF were chosen as 20% based on the revealed physicochemical properties (See "Results"). For the operation, the mice were anesthetized with 3% isoflurane in a mixture of $N_2O : O_2$ (70 : 30). The body temperature was maintained at 37.0 ± 0.5°C using a heating pad. The abdomen was shaved and sterilized with iodine and alcohol solution. Then, the peritoneal cavity was opened with a 3 cm long-abdominal midline incision and the cecum was identified and abraded with a 1 cm^2-defect by rubbing with a sterile toothbrush. When petechial was visualized, abrasion was stopped. Subsequently, for the MET@CA-AF or CA-AF groups, cecal surfaces were covered by 2 × 2 cm-sized rectangular films with an aids of normal saline spray. The same procedures were executed for the OP group except the lack of the film application. Pri-

or to the closure of the operation wound, the starch powder was poured on abrasion site for encouraging the firm adhesion. For the suture of the wound, 4~0 black silk was used. After the operation, all mice were transferred to home cages and maintained with *ad libitum* throughout the experiment.

Adhesion scoring

At postoperative day (POD) 14, the animals were sacrificed with an intraperitoneal injection of urethane (2 mL/kg). The abdominal cavity was opened via a U-shaped abdominal incision. The severity was assessed by the standard adhesion scoring system in accordance with Lauder's method [23]. The assessment was performed by the 2 investigators blinded to the operation. Adhesions were graded from 0 to 5 : 0, no adhesion; 1, one thin filmy adhesion; 2, more than one thin adhesion; 3, thick adhesion with focal point; 4, thick adhesion with planar attachment or more than one thick adhesion with focal point; and 5, very thick vascularized adhesion or more than one planar adhesion.

Histologic procedure

For histological examination, specimens were collected from the sacrificed mice immediately after macroscopic examination. The obtained specimen, a sandwich of tissue that consists of skin and abdominal wall on one side, bowel on the other side, and adhesive tissue connecting the two in between, were then cut into small pieces by 1 × 1 cm and fixed for 24 h in 4% paraformaldehyde diluted in PBS. Then, the fixed tissue was dehydrated with increasing concentrations of alcohol and embedded in paraffin wax. The paraffin blocks were cut into 5 μm-thick sections with tissue microtome (RM2255; Leica, Nussloch, Germany). Randomly selected 2 tissue sections of different groups were deparaffinized with xylene and rehydrated with decreasing concentrations of alcohol. The sections were stained with H-E and Masson's trichrome staining in accordance with the methods described elsewhere [24-26]. The tissue sections were acquired at 200× magnification using a digital camera connected with a light microscope (DM4; Leica). The mean of adhesion interface thickness was measured with random selection of foci of examination (n = 20 per high power field), followed by calculation with an aid of an image analysis system (Image J software Ver. 1.37, National Institutes of Health).

Immunofluorescence

Randomly selected, 2 tissue sections of different groups were deparaffinized and rehydrated. The sections were subjected to an antigen retrieval step using the Target retrieval solution® (DAKO, Glostrup, Denmark) in accordance with the manufacturer's protocol. After 3-times wash in PBS, the tissues were incubated with primary antibodies (mouse anti-collagen-I and rabbit anti-vimentin), diluted in PBS at a ratio of 1 : 250, for 24 h at 4°C. The tissues were washed with PBS and incubated with secondary antibodies (goat anti-mouse Cy2 and anti-rabbit Cy3), diluted in PBS at a ratio of 1 : 250, for 2 h at 24°C. All the secondary antibodies were purchased from Santa Cruz Biotechnology (Dallas, TX, USA). The tissues were mounted with 4′, 6-diamidino-2-phenylindole (DAPI)-contained mounting medium (Santa Cruz Biotechnology, Santa Cruz, CA, USA) and examined with a confocal laser scanning microscope (LSM700, Zeiss, Munchen, Germany). The resulting DAPI- and vimentin-immunopositive cells, surrounded by collagen-I fluorescence, were considered as activated myofibroblast and were counted in the captured images showing randomly selected high power fields (n = 3 per tissue) and averaged per individual group.

Statistical analysis

All the results are expressed as mean ± standard deviation (SD). Comparisons of the data from the different groups were performed with one-way analysis of variance (ANOVA, PASW Statistics v. 18, SPSS Inc., Chicago, IL, USA). Differences with $p < 0.05$ were considered statistically significant.

RESULTS

General characteristics of MET@CA-AF

The manufactured MET@CA-AF was transparent, moderately flexible, and rigid (Fig. 1A). The resulting chemical formula of MET@CA-AFs after crosslinking reaction and predicted releasing dynamics of MET are illustrated in Fig. 1B. With increased crosslinking (from C0 to C20), the films became less flexible and more rigid in the manual examination. Upon water spraying, the films became soften and sticky, thus enabling their attachment on biological surfaces like skin of dorsal hand and injured cecal surface.

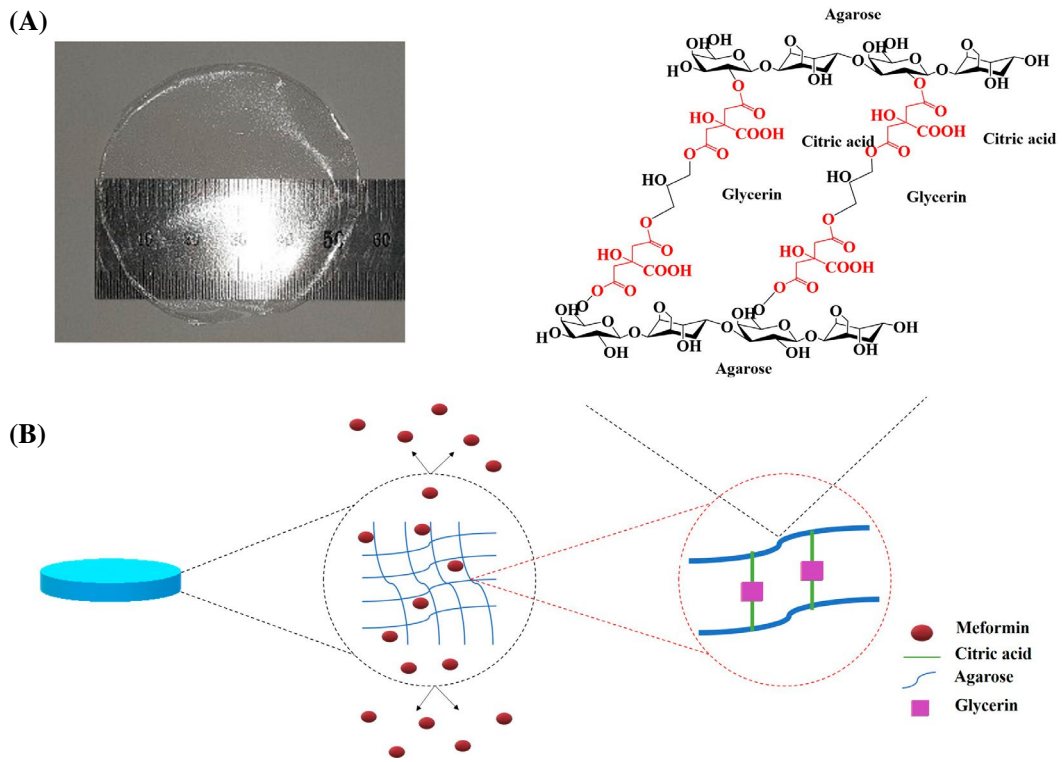

Fig. 1. The novel synthesized MET@CA-AF. (A) The macroscopic appearance of MET@CA-AF. (B) Chemical formula of MET@CA-AFs after cross-linking reaction and the predicted releasing dynamics of MET from MET@CA-AF.

Physicochemical properties of MET@CA-AF

The FT-IR spectroscopy was employed to confirm the cross-linking reaction. As shown in Fig. 2A, although the FT-IR spectra of C0, C10, and C20 were similar, the indicator of ester linkage (C=O), visible trough at 1730 cm^{-1}, was only present in the spectrogram of the C10 and C20, but not C0. In addition, the trough of C20 was deeper than that of C10. These results demonstrated that esterification reaction had indeed occurred during the crosslinking process and its strength depended on the CA concentration. Next, we quantified the water retention abilities by calculating the swelling ratio of different CA-AFs. When agarose chains are cross-linked, their freedom of movement is reduced, thereby reducing the amount of water absorbed upon soaking [27]. As shown in Fig. 2B, reduction in the water absorption after 24 h was observed in the films cross-linked with CA, which occurred in a concentration-dependent manner. Subsequently, we evaluated the *in vitro* biodegradability of different CA-AFs by immersing into PBS while maintaining 37°C, measuring the mechanical resistances against the environment inside the peritoneal cavity. The time-dependent weight reduction was reduced in the C20 when compared with either the C0 or C10 (Fig. 2C). We postulated that C20 composition is able to keep structural stability maintaining over 70% of the weight estimated at the time of implantation. In addition, the hydrophilicity of CA-AFs was elucidated as a function of cross-linking strength. As shown in the results of contact angle measurement (Fig. 2D), the films became less hydrophilic with increased cross-linking (from C0 to C20). However, the level of hydrophilicity of C20 was still higher than that of Surgiwrap® used as a positive control. Given that the Surgiwrap® lacks hydrophilicity and frequently renders the fixation suture on wound site to be needed in clinic [8], all of CA-AFs, even a C20 composite, are expected to exert higher biocompatibility. Finally, as the prepared films could be used as implants, *in vitro* drug release study was performed at pH 7.4. The *in vitro* MET release profile is presented in Fig. 2E. An initial burst of ~20 to 60% release of MET was observed from all films until up to 30 min. After that, controlled releasing dynamics of MET were observed from all composites. Consistent with the fact that the swelling of hydrogel film increased its thickness, retardation of

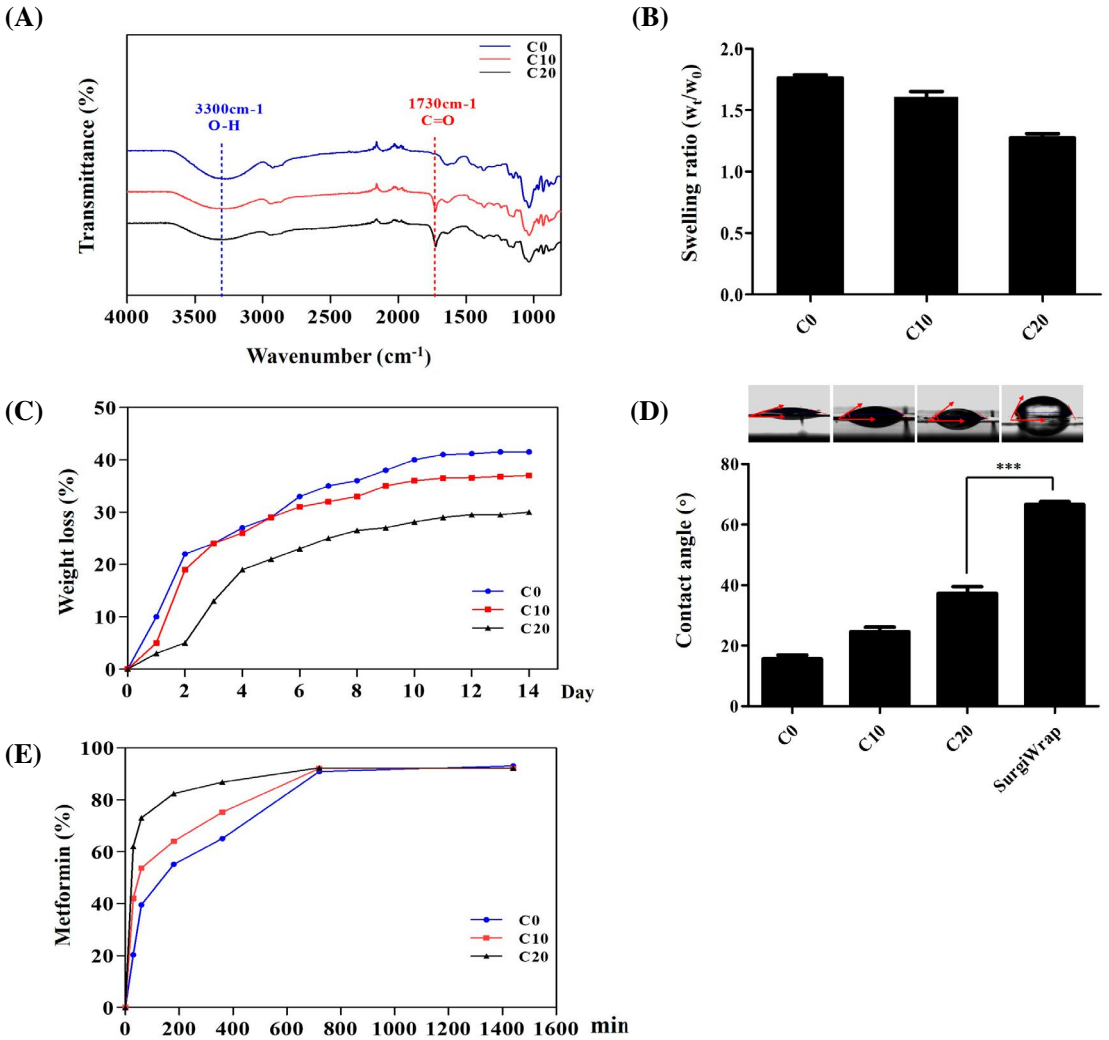

Fig. 2. Physicochemical properties of the CA-AFs with different concentrations of CA and MET@CA-AF. (A) FT-IR spectra with indicated esterification, (B) swelling properties, (C) *in vitro* degradation properties, (D) hydrophilicity, and (E) *in vitro* MET-releasing properties of CA-AFs cross-linked with different concentrations of CA. In graphs of (B) and (D), data were represented as mean±S.D ($p^{***} < 0.001$ between the indicated samples).

MET release was more apparent in C20 than in other composites. Hence, C20 was chosen as the best composite of MET@CA-AF for *in vivo* studies.

Preventive effect of MET@CA-AF in rat model of PAA

At POD 14, all survived mice received laparotomy as described at the methods section. The mean adhesion scores for all groups are shown in Table 1. With an exception of 7 mice that did not recover from anesthesia or died after surgery, all animals were in a good health during the follow-up period. Overall, the comparison of all studied groups revealed statistically significant differences. In contrast to the CTRL group that showed no adhesions at all, severe adhesions (grade 4 and 5) were generated in the OP group. However, CA-AF group and MET@CA-AF group were associated with significantly lower adhesion scores when compared to the OP group (2.3 ± 0.82 and 0.33 ± 0.52 vs. 4.4 ± 0.55, $p^{***} < 0.001$). Interestingly, the MET@CA-AF group showed significantly lower adhesion scores when compared to the CA-AF group ($p^{\dagger\dagger\dagger} < 0.001$). Representative laparoscopic images (Fig. 3A) demonstrated a generation of wide and well-developed adhesions in between the abdominal wall and the cecum in the OP group, an apparent minimization of the adhesion in the CA-AF group,

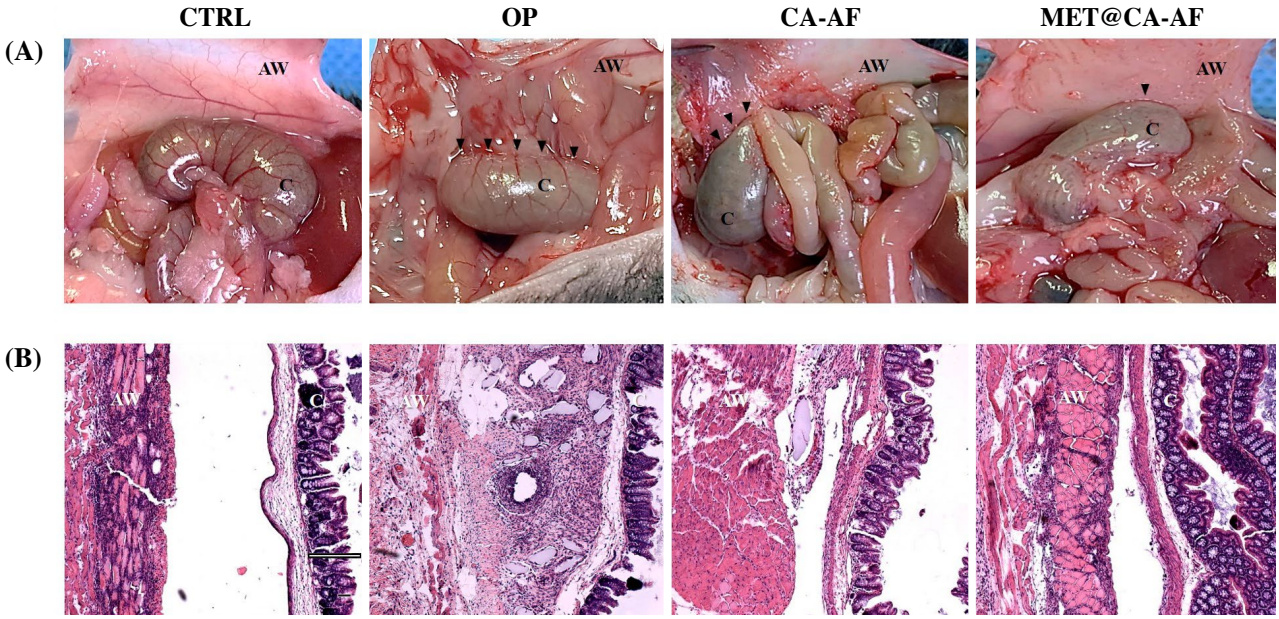

Fig. 3. Attenuation of gross findings associated with postoperative abdominal adhesion by MET@CA-AF. (A) Representative laparoscopic images obtained at POD 14. The wide and well-developed adhesions are indicated with black arrowheads, the abdominal wall is indicated as AW, and the cecum is indicated as C. (B) H-E stained tissue samples involving the adhesive lesion. Scale bar = 100 μm.

and the further exaggeration in this extent in the MET@CA-AF. To give a histopathological insight for preventive role of these films on PAA, tissue samples consisting of abdominal wall and cecum were stained with H-E (Fig. 3B). While the space between abdominal wall and cecum was visible in CTRL group, the space was occupied by thick fibrous tissues in the OP group. The adhesion was also observed in the CA-AF group, although the foci was tiny and partial. More interestingly, none of the adhesions was observed in the MET@CA-AF group, indicating that the injured abdominal wall and cecum were fully recovered. To measure the adhesion interface, Masson's trichrome staining was adopted for clear discrimination of collagen fiber. As shown in Fig. 4A and 4B, the adhesion interface of the CA-AF group was significantly narrower than that of the OP group (142.6 ± 31.7 vs. 375.3 ± 90.1 μm, p*** < 0.001). Remarkably, the adhesion interface was further diminished thus reaching nearly zero in the MET@CA-AF group (4.0 ± 0.6, $p^{\dagger\dagger\dagger}$ < 0.001 vs. CA-AF group).

Table 1. Attenuation of PAA severity by MET@CA-AF. Adhesions are graded from 0 to 5 : 0, no adhesion; 1, one thin filmy adhesion; 2, more than one thin adhesion; 3, thick adhesion with focal point; 4, thick adhesion with planar attachment or more than one thick adhesion with focal point; and 5, very thick vascularized adhesion or more than one planar adhesion. Data are represented as a mean ± S.D.

Adhesion	CTRL	OP	CA-AF	MET@CA-AF
0	8	0	0	4
1	0	0	1	2
2	0	0	2	0
3	0	0	3	0
4	0	3	0	0
5	0	2	0	0
Death	0	3	2	2
Mean ± S.D	0	4.4 ± 0.55	2.3 ± 0.82***	0.33 ± 0.52***,†††

***p < 0.001 vs OP, †††p < 0.001 vs CA-AF

Attenuation of myofibroblast activation by MET@CA-AF

To evaluate whether activation of myofibroblast, a key cellular culprit of extracellular matrix (ECM) deposition, can be attenuated by the MET@CA-AF, thereby facilitating prevention, IF using antibodies against collagen-I and vimentin was employed (Fig. 4C and 4D). The result showed that the activated myofibroblasts ($DAPI^+$ $vimentin^+$ cells surrounded by collagen-I^+ fluorescence; Fig. 4C) were abundant in the OP group. However, the number of activated myofibroblasts was markedly reduced in the CA-AF group compared to the OP group (25.2 ± 2.6 vs. 51.3 ± 14.3, p** < 0.01). Moreover, this reduction was bigger in

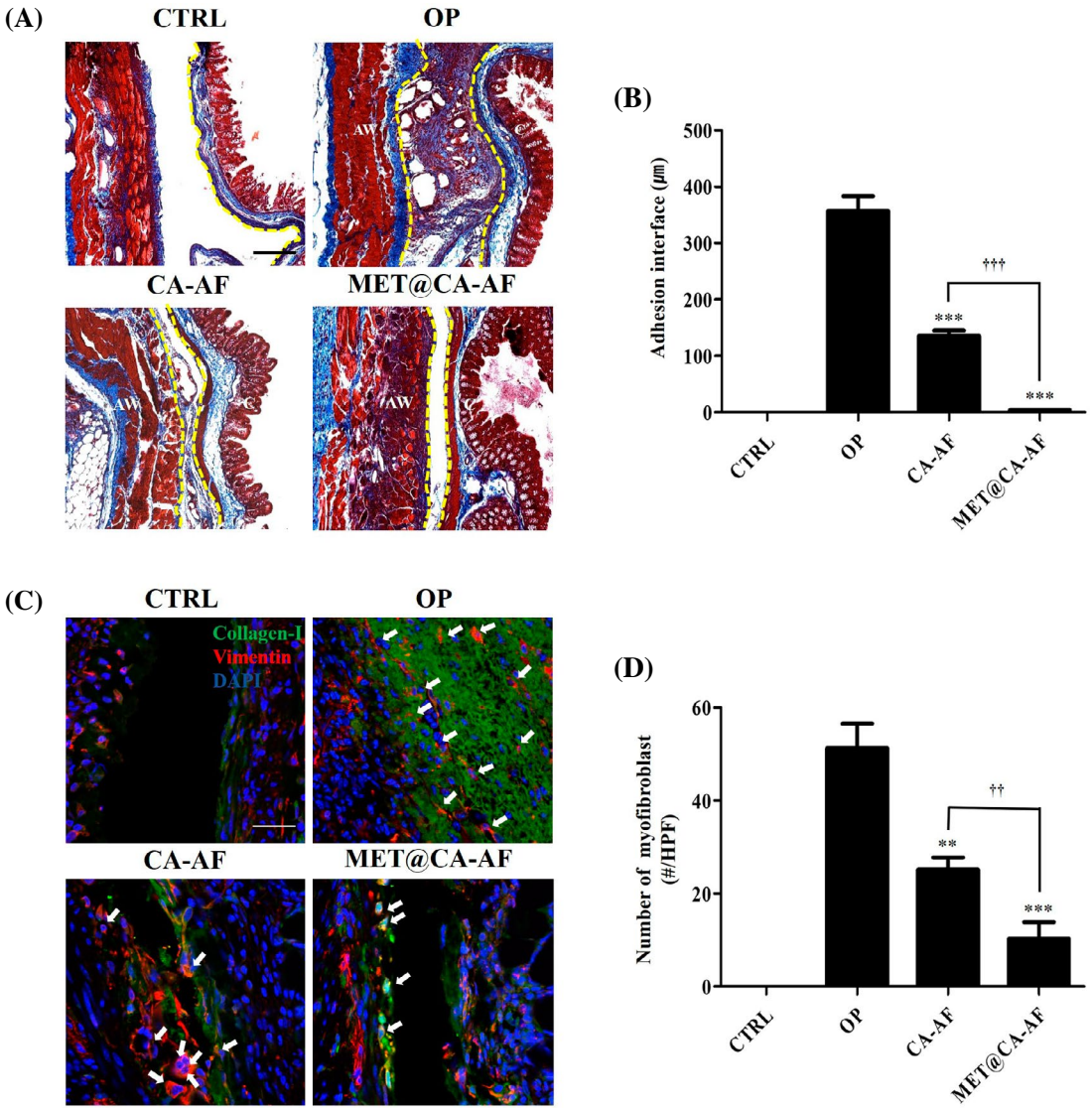

Fig. 4. Inhibition of the adhesion interface formation and myofibroblast activation by MET@CA-AF. (A) Representative Masson's trichrome-stained tissue samples involving the adhesive lesion. Scale bar = 100 μm. (B) Quantitative graphs showing the averaged thicknesses of adhesion interface of different groups. Data are represented as mean ± S.D ($p^{***} < 0.001$ vs. OP group. $p^{†††} < 0.001$ vs. CA-AF group). (C) Representative images of immunofluorescence for detecting activated myofibroblast, which is depicted as $DAPI^+$ $vimentin^+$ cells surrounded by collagen-I^+ fluorescence (indicated with white arrows). Scale bar = 50 μm. (D) Quantitative graphs showing the average number of activated myofibroblasts of different groups. Data are represented as mean ± S.D ($p^{**} < 0.01$ and $p^{***} < 0.001$ vs. OP group; $p^{††} < 0.01$ vs. CA-AF group).

the MET@CA-AF compared to the CA-AF group (10.3 ± 8.87, $p^{††} < 0.01$). This result suggests that MET, conferred the additive role on CA-AF-mediated PAA prevention by inhibiting myofibroblast activation.

DISCUSSION

To date, PAA remains a common and serious postsurgical problem, which results in considerable morbidity, mortality, and economic burden [1,28]. The most serious complication of PAA is bowel obstruction, chronic or recurrent abdominal pain, and infertility in women [3,29]. A variety of pharmaceutical treatments have been proposed to reduce the PAA risks, including systemic or intraperitoneal glucocorticoids [30], anticoagulants [31], antihistamines [32], nonsteroidal anti-inflammatory agents [33], high mo-

lecular weight dextran [34], and fibrinolytic agents [35]. Unfortunately, none of them has proven to be sufficiently efficacious in humans.

Despite the complexity of PAA pathogenesis, accumulating evidences have revealed that fibrin formation derived by multi-organ irritation is the key initial step [36]. The endogenous fibrinolytic system inside the peritoneal cavity inhibits the fibrin deposition, thus maintaining the balance between coagulation and fibrinolysis in normal condition. However, once abdominal surgery is performed, the balance might be disrupted and a coagulation process may occur. The resulting fibrin deposits become a scaffold of fibrotic tissue. In fact, fibroblasts migrates to and proliferates in the fibrin matrix, producing ECM components such as collagen-I [37]. Generally, if compensatory fibrinolysis does not occur within POD 7, the temporary fibrin matrix can be consolidated and gradually organized with the aids of accompanying angiogenesis and neurogenesis [38].

As the fibrin formation has been known to be an initial key step towards PAA pathogenesis, many studies have been performed in an attempt to block the fibrin formation [39]. The most commonly used strategy is site-specific or broad-coverage barriers. The barriers, which are commonly produced as hydrogels, supply temporal physical interface preventing adhesions between the parietal and the visceral peritoneum [40]. Despite all efforts, all purely physical barriers failed to protect against PAA because they fail to address the basic biological problems including the difficulties in the control of their biocompatibility and biodegradability.

We envisioned that a multi-functional agent locally delivered by a biocompatible, biodegradable, and muco-adhesive barrier material could be useful in reducing PAA severity. Here, we report the novel form of agarose-based barrier for the prevention of PAA. In detail, chemically crosslinked AF were first fabricated with the different concentrations of CA yielding the CA-AF and their physicochemical properties were measured. Next, MET, a commercially available anti-diabetic drug, was loaded inside, thus yielding the MET@CA-AF. MET has been shown to reduce transforming growth factor-β-induced extracellular matrix protein production in fibroblasts derived from nasal polyps [41]. Furthermore, MET prevented airway remodeling in mouse models of bronchial asthma, suggesting a potential anti-fibrotic property [42]. We therefore selected MET as a candidate drug to be loaded within the novel synthesized barrier, which was used in mouse models of PAA. The results showed that applications of CA-AF or MET@CA-AF for 14 days significantly attenuated the severity of PAA. Importantly, the MET@CA-AF produced better protection against PAA then the CA-CF.

A major limitation of this study is that we could not rule out the possibility that MET might exert protective effect on PAA by another mechanism. In fact, numerous possible targets of MET exist in the pathogenesis of PAA. For example, various experimental studies have shown that MET has antioxidant [43], anti-inflammatory [44], and fibrinolytic properties [45], all of which are related to PAA formation and prevention. Thus, based on the diverse biological properties of MET, approaches for unveiling other therapeutic mechanisms and specific molecular targets might be needed in the context of preventive effects of MET@CA-AFs on PAA.

REFERENCES

1. Tabibian N, Swehli E, Boyd A, Umbreen A, Tabibian JH. Abdominal adhesions: a practical review of an often overlooked entity. Ann Med Surg (Lond). 2017;15:9-13.
2. Van Goor H. Consequences and complications of peritoneal adhesions. Colorectal Dis. 2007;9:25-34.
3. Cohen Z, Senagore AJ, Dayton MT, Koruda MJ, Beck DE, Wolff BG, et al. Prevention of postoperative abdominal adhesions by a novel, glycerol/sodium hyaluronate/carboxymethylcellulose-based bioresorbable membrane: a prospective, randomized, evaluator-blinded multicenter study. Dis Colon Rectum. 2005;48:1130-9.
4. Tabchouri N, Dussart D, Giger-Pabst U, Michot N, Marques F, Khalfallah M, et al. Only surgical treatment to be considered for adhesive small bowel obstruction: a new paradigm. Gastroenterol Res Pract. 2018;2018:9628490.
5. Lin LX, Yuan F, Zhang HH, Liao NN, Luo JW, Sun YL. Evaluation of surgical anti-adhesion products to reduce postsurgical intra-abdominal adhesion formation in a rat model. PLoS One. 2017;12:e0172088.
6. Yang Y, Liu X, Li Y, Wang Y, Bao C, Chen Y, et al. A postoperative anti-adhesion barrier based on photoinduced imine-crosslinking hydrogel with tissue-adhesive ability. Acta Biomater. 2017;62:199-209.
7. Wu J, Li P, Dong C, Jiang H, Bin X, Gao X, et al. Rationally designed synthetic protein hydrogels with predictable mechanical properties. Nat Commun. 2018;9:620.
8. Lee CH, Kim H, Han IW, Kim SM, Kwak BS, Baik YH, et

al. Effect of polylactic film (Surgi-Wrap) on preventing postoperative ileus after major hepato-pancreato-biliary surgery. Ann Hepatobiliary Pancreat Surg. 2016;20:191-6.
9. Rocca A, Aprea G, Surfaro G, Amato M, Giuliani A, Paccone M, et al. Prevention and treatment of peritoneal adhesions in patients affected by vascular diseases following surgery: a review of the literature. Open Med (Wars). 2016;11:106-14.
10. Lang R, Baumann P, Schmoor C, Odermatt EK, Wente MN, Jauch KW. A-Part Gel, an adhesion prophylaxis for abdominal surgery: a randomized controlled phase I-II safety study [NCT00646412]. Ann Surg Innov Res. 2015;9:5.
11. Yeo Y, Kohane DS. Polymers in the prevention of peritoneal adhesions. Eur J Pharm Biopharm. 2008;68:57-66.
12. Maciver AH, McCall MD, Edgar RL, Thiesen AL, Bigam DL, Churchill TA, et al. Sirolimus drug-eluting, hydrogel-impregnated polypropylene mesh reduces intra-abdominal adhesion formation in a mouse model. Surgery. 2011;150:907-15.
13. Hoare TR, Kohane DS. Hydrogels in drug delivery: Progress and challenges. Polymer. 2008;49:1993-2007.
14. Leonelli F, La Bella A, Migneco LM, Bettolo RM. Design, synthesis and applications of hyaluronic acid-paclitaxel bioconjugates. Molecules. 2008;13:360-78.
15. Chowdhury SM, Hubbell JA. Adhesion prevention with ancrod released via a tissue-adherent hydrogel. J Surd Res. 1996;61:58-64.
16. Grolman JM, Singh M, Mooney DJ, Eriksson E, Nuutila K. Antibiotic-containing agarose hydrogel for wound and burn care. J Burn Care Res. 2019;40:900-6.
17. Colquhoun AJ, Venier NA, Vandersluis AD, Besla R, Sugar LM, Kiss A, et al. Metformin enhances the antiproliferative and apoptotic effect of bicalutamide in prostate cancer. Prostate Cancer Prostatic Dis. 2012;15:346-52.
18. Al-Dwairi A, Alqudah M, Al-Shboul O, Alfaqih M, Alomari D. Metformin exerts anti-inflammatory effects on mouse colon smooth muscle cells *in vitro*. Exp Ther Med. 2018;16:985-92.
19. Zucca P, Fernandez-Lafuente R, Sanjust E. Agarose and its derivatives as supports for enzyme immobilization. Molecules. 2016;21:E1577.
20. Wong RSH, Dodou K. Effect of drug loading method and drug physicochemical properties on the material and drug release properties of poly (Ethylene Oxide) hydrogels for transdermal delivery. Polymers (Basel). 2017;9:E286.
21. Council NR. Guide for the care and use of laboratory animals. 8th ed. Washington, DC: The National Academies Press; 2011.
22. Gao Q, Wei G, Wu Y, Yao N, Zhou C, Wang K, et al. Paeoniflorin prevents postoperative peritoneal adhesion formation in an experimental rat model. Oncotarget. 2017;8:93899-911.
23. Lauder CI, Garcea G, Strickland A, Maddern GJ. Use of a modified chitosan-dextran gel to prevent peritoneal adhesions in a rat model. J Surg Res. 2011;171:877-82.
24. Jeong JH, Kim DK, Lee NS, Jeong YG, Kim HW, Kim JS, et al. Neuroprotective effect of nortriptyline in overt hepatic encephalopathy through attenuation of mitochondrial dysfunction. ASN Neuro. 2018;10:1759091418810583.
25. Fischer AH, Jacobson KA, Rose J, Zeller R. Hematoxylin and eosin staining of tissue and cell sections. CSH protoc. 2008;2008:pdb.prot4986.
26. Wu Q, Wang N, He T, Shang J, Song L, Yang X, et al. Thermosensitive hydrogel containing dexamethasone micelles for preventing postsurgical adhesion in a repeated-injury model. Sci Rep. 2015;5:13553.
27. Ahmed EM. Hydrogel: Preparation, characterization, and applications: A review. J Adv Res. 2015;6:105-21.
28. Moris D, Chakedis J, Rahnemai-Azar AA, Wilson A, Hennessy MM, Athanasiou A, et al. Postoperative abdominal adhesions: clinical significance and advances in prevention and management. J Gastrointest Surg. 2017;21:1713-22.
29. Rajab TK, Ahmad UN, Kelly E. Implications of late complications from adhesions for preoperative informed consent. J R Soc Med. 2010;103:317-21.
30. Hosseini A, Akhavan S, Menshaei M, Feizi A. Effects of streptokinase and normal saline on the incidence of intra-abdominal adhesion 1 week and 1 month after laparotomy in rats. Adv Biomed Res. 2018;7:16.
31. Charboneau AJ, Delaney JP, Beilman G. Fucoidans inhibit the formation of post-operative abdominal adhesions in a rat model. PLoS One. 2018;13:e0207797.
32. Brüggmann D, Tchartchian G, Wallwiener M, Münstedt K, Tinneberg HR, Hackethal A. Intra-abdominal adhesions: definition, origin, significance in surgical practice, and treatment options. Dtsch Arztebl Int. 2010;107:769-75.
33. Rouhani A, Tabrizi A, Ghavidel E. Effects of non-steroidal anti-inflammatory drugs on flexor tendon rehabilitation after repair. Arch Bone Jt Surg. 2013;1:28-30.
34. Rosenberg SM, Board JA. High-molecular weight dextran in human infertility surgery. Am J Obstet Gynecol. 1984;148:380-5.
35. Topal E, Ozturk E, Sen G, Yerci O, Yilmazlar T. A comparison of three fibrinolytic agents in prevention of intra-abdominal adhesions. Acta Chir Belg. 2010;110:71-5.
36. Molinas CR, Binda MM, Manavella GD, Koninckx PR. Adhesion formation after laparoscopic surgery: what do we know about the role of the peritoneal environment? Facts Views Vis Obgyn. 2010;2:149-60.
37. Frantz C, Stewart KM, Weaver VM. The extracellular matrix at a glance. J Cell Sci. 2010;123:4195-200.
38. Kanno Y. The role of fibrinolytic regulators in vascular dys-

function of systemic sclerosis. Int J Mol Sci. 2019;20:E619.
39. Irkorucu O, Ferahköşe Z, Memiş L, Ekinci O, Akin M. Reduction of postsurgical adhesions in a rat model: a comparative study. Clinics (Sao Paulo). 2009;64:143-8.
40. Thornton MH, Johns DB, Campeau JD, Hoehler F, DiZerega GS. Clinical evaluation of 0.5% ferric hyaluronate adhesion prevention gel for the reduction of adhesions following peritoneal cavity surgery: open-label pilot study. Hum Reprod. 1998;13:1480-5.
41. Park IH, Um JY, Hong SM, Cho JS, Lee SH, Lee SH, et al. Metformin reduces TGF-β1-induced extracellular matrix production in nasal polyp-derived fibroblasts. Otolaryngol Head Neck Surg. 2014;150:148-53.
42. Sato N, Takasaka N, Yoshida M, Tsubouchi K, Minagawa S, Araya J, et al. Metformin attenuates lung fibrosis development via NOX4 suppression. Respir Res. 2016;17:107.
43. Dehkordi AH, Abbaszadeh A, Mir S, Hasanvand A. Metformin and its anti-inflammatory and anti-oxidative effects; new concepts. J Renal Inj Prev. 2019;8:54-61.
44. Saisho Y. Metformin and inflammation: its potential beyond glucose-lowering effect. Endocr Metab Immune Disord Drug Targets. 2015;15:196-205.
45. Markowicz-Piasecka M, Huttunen K, Mateusiak L, Mikiciuk-Olasik E, Sikora J. Is metformin a perfect drug? updates in pharmacokinetics and pharmacodynamics. Curr Pharm Des. 2017;23:2532-50.